



Investigating Nucleation Using the Phase-Field Method

Frigyes Podmaniczky,^{1*} Gyula I. Tóth,^{1,2} Tamás Pusztai,¹ and László Gránásy^{1,3*}

Abstract | The first order phase transitions, like freezing of liquids, melting of solids, phase separation in alloys, vapor condensation, etc., start with nucleation, a process in which internal fluctuations of the parent phase lead to formation of small seeds of the new phase. Owing to different size dependence of (negative) volumetric and (positive) interfacial contributions to work of formation of such seeds, there is a critical size, at which the work of formation shows a maximum. Seeds that are smaller than the critical one decay with a high probability, while the larger ones have a good chance to grow further and reach a macroscopic size. Putting it in another way, to form the bulk new phase, the system needs to pass a thermodynamic barrier via thermal fluctuations. When the fluctuations of the parent phase alone lead to transition, the process is called homogeneous nucleation. Such a homogeneous process is, however, scarcely seen and requires very specific conditions in nature or in the laboratory. Usually, the parent phase resides in a container and/or it incorporates floating heterogeneities (solid particles, droplets, etc.). The respective foreign surfaces lead to ordering of the adjacent liquid layers, which in turn may assist the formation of the seeds, a process termed heterogeneous nucleation. Herein, we review how the phase-field techniques contributed to the understanding of various aspects of crystal nucleation in undercooled melts, and its role in microstructure evolution. We recall results achieved using both conventional phase-field techniques that rely on spatially averaged (coarse grained) order parameters in capturing the phase transition, as well as molecular scale phase-field approaches that employ time averaged fields, as happens in the classical density functional theories, including the recently developed phase-field crystal models.

Driving force: It is the volumetric grand free energy difference between the crystal and the liquid, which is negative, $\Delta\omega < 0$, in the undercooled state.

1 Introduction

The crystalline freezing, ideally, of pure liquids cooled below their melting point starts with *nucleation*, a process during which crystal-like fluctuations appear, whose size exceeds a critical value, determined by the solid-liquid interface free energy (γ_{SL}) and the thermodynamic **driving force** ($\Delta\omega$) of crystallization. Those crystal-like fluctuations that are larger than the critical size tend to grow to a macroscopic size, whereas the smaller

ones decay with a high probability, although clusters momentarily on one of the sides of the maximum can move to the other via stochastically capturing/releasing molecules. The critical size fluctuation of the new phase is termed *nucleus*.

Since the description of crystal nucleation has a long history, addressed in excellent reviews,¹⁻³ this review is limited to contributions from phase-field modeling. First, we briefly recall some essential notions, which can be easily introduced

¹Institute for Solid State Physics and Optics, Wigner Research Centre for Physics, H-1525 Budapest, Hungary.

²Department of Physics and Technology, University of Bergen, Allégaten 55, N-5007 Bergen, Norway.

³BCAST, Brunel University, Uxbridge, Middlesex, UB8 3PH, UK.

*granasy.laszlo@wigner.mta.hu
*podmaniczky.frigyes@wigner.mta.hu

in the framework of the classical nucleation theory (CNT).¹

1.1 The classical nucleation theory

The classical nucleation theory relies on a simplified view of the critical fluctuation: it is assumed to be a small spherical domain of the bulk crystalline phase inside the bulk liquid phase, with a sharp interface in between. Predictions of theory are based on evaluation of the negative volumetric and positive interfacial energies that determine the total excess energy, i.e. the work of formation of the nucleus.

Homogeneous nucleation: Work of formation of a spherical crystalline domain is expressed as a sum of a negative volumetric and a positive interfacial term as $W_{\text{hom}} = (4\pi/3)R^3\Delta\omega + 4\pi R^2\gamma_{\text{SL}}$, where R is the radius of the sphere. For small sizes the positive surface term, while for the large ones the negative volumetric term dominates. Thus, the work of formation shows a maximum as a function of size, where $W_{\text{hom}}^* = (16\pi/3)\gamma_{\text{SL}}^3/\Delta\omega^2$ and $R^* = -2\gamma_{\text{SL}}/\Delta\omega$ are the free energy and radius corresponding to this maximum, defining the critical fluctuation or nucleus. It is easy to see that R^* decreases if the driving force (undercooling) increases. Since it is assumed that these “heterophase” fluctuations originate from the internal density/structural fluctuation of an ideally pure liquid, this process is known as *homogeneous nucleation*.

In the CNT, the formation rate of critical fluctuations is calculated considering single molecule attachment and detachment to the clusters. The master equations that describe the time evolution of the cluster population is written as follows:¹

$$\dot{N}_1 = a_2^- N_2 - a_1^+ N_1 + \sum_{n>1} (a_n^- N_n - a_{n-1}^+ N_{n-1}) \quad (1a)$$

$$\dot{N}_n = a_{n-1}^+ N_{n-1} + a_{n+1}^- N_{n+1} - (a_n^+ + a_n^-) N_n, \text{ for } n > 1. \quad (1b)$$

Here, N_n is the number of clusters that consist of n atoms/molecules, $a_n^+ = O_n \Gamma \exp\{- (W_{n+1} - W_n)/2kT\}$ and $a_n^- = O_{n-1} \Gamma \exp\{- (W_{n-1} - W_n)/2kT\}$ are the molecule attachment and detachment frequencies, $O_n = 4n^{2/3}$ the number of sites on the surface of the n -molecule cluster, to which a molecule can be attached, $\Gamma = 6D/\lambda^2$ determines the time scale of molecule attachment/detachment, where D is the self-diffusion coefficient (often related to the viscosity via the Stokes-Einstein relationship), and λ the molecular jump distance. W_n is the free energy of formation of

an n -molecule cluster, k is Boltzmann's constant, and T the temperature. Solving these equations numerically, after a transient period of length $\tau \approx K\lambda^2 kT(n^*)^{2/3}/(Dv_m \Delta\omega)$, where K is a geometrical factor, n^* the number of molecules in the critical fluctuation, and v_m the molecular volume, a steady state *nucleation rate* (net number of critical fluctuations formed in unit volume and unit time) of form

$$J_{\text{ss}} = \frac{1}{\left\{ \sum_{n=1}^{\infty} (a_n^+ N_{eq,n})^{-1} \right\}} \approx \frac{J_0 \exp\{-W_{\text{hom}}^*/kT\}}{Z} \quad (2)$$

is established,¹ where the equilibrium number density of n -molecule clusters is $N_{eq,n} = \rho_0 \exp\{-W_n/kT\}$, $J_0 = \rho_0 O_{n^*} \Gamma Z$ is the pre-exponential factor of nucleation, ρ_0 the number density of the monomers (molecules). Here $Z = \{|d^2 W_{\text{hom}} / dn^2|_{n^*}\}^{1/2}$ is the Zeldovich factor that takes the dissolution of critical clusters into account. Experiments on oxide glasses indicate that the magnitude of the classical prefactor J_0 is reasonable^{1,4,5}, a conclusion also supported by comparison with advanced theory.⁶⁻⁸ A comparison with molecular dynamics simulations, however, indicates that J_0 might be too low by two orders of magnitude.⁹ Extensions of the classical kinetic approach to cluster coagulation and splitting have also been explored.^{10,11}

Heterogeneous nucleation: In practice, the formation of the crystallike fluctuations is assisted by various kinds of heterogeneities (e.g., container walls, floating particles, molecular impurities, etc.), which reduce the height of the nucleation barrier significantly ($W_{\text{het}}^* < W_{\text{hom}}^*$), making thus the appearance of nuclei easier. The spherical cap model captures this in the following manner: assume that the foreign particles are much larger than the nuclei, and are distributed homogeneously in the undercooled fluid and they are bound by flat walls. A flat solid-liquid interface can only be in equilibrium with the wall if the Young-Laplace equation holds: i.e., $\gamma_{WL} = \gamma_{WS} + \gamma_{SL} \cos(\psi)$, where γ_{WL} and γ_{WS} are the wall-liquid and wall-solid interface free energies, respectively, while ψ is the equilibrium contact angle or wetting angle. In the presence of such a wall, the classical theory predicts a critical fluctuation that has the shape of a spherical cap (that fraction of the homogeneous nucleus, which realizes the contact angle; see Fig. 1). Accordingly, the free energy of formation is $W_{\text{het}}^* = W_{\text{hom}}^* f(\psi)$, where $f(\psi) = 1/4 [2 + \cos(\psi)] \{1 - \cos(\psi)\}^2$ is the catalytic potency factor. For small

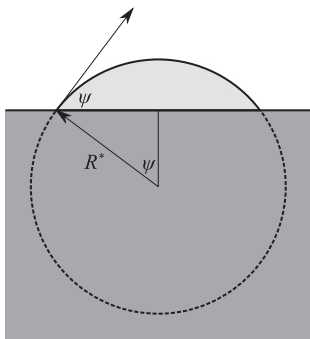


Figure 1: The “spherical cap” approach used to describe heterogeneous nucleation on a flat substrate (dark gray). Imagine a sphere of radius R^* that corresponds to the homogeneous nucleus. Position this sphere in a way that its intersection with the surface realizes the required contact angle ψ (determined by the Young-Laplace equation, see text). The heterogeneous nucleus is then the spherical cap (light gray) on top of the substrate.

contact angles (good wetting), $f(\psi)$ can be small, lowering the nucleation barrier significantly. On the surface of the spherical cap in contact with the liquid, the number of sites to which molecules can be attached is $O_n = 2\{1 - \cos(\psi)\}n^{2/3}$. Considering that only those molecules can take part in heterogeneous nucleation that are adsorbed on the surface of the heterogeneities, the steady state nucleation rate may be expressed as $J_{SS,het} = x_A^{1/2}\{1 - \cos(\psi)\}/f(\psi)^{1/2}J_0 \exp\{-W_{hom} * f(\psi)/kT\}$.^{12,13} Here, x_A is the fraction of molecules adsorbed on the surface of heterogeneities. This approach has been modified for cases of various substrate geometries including spherical particles, rough surfaces, nucleation in depressions, etc.¹⁴

1.2 Free growth limited mode of particle induced freezing

Greer and coworkers proposed a simple but rather successful model for describing particle induced solidification in undercooled liquids.^{15,16} The foreign particles are assumed to be of cylindrical form of radius R , with ideally wetting circular faces ($\psi=0$), and non-wetting sides ($\psi=\pi$). These idealized particles remain dormant until a critical undercooling is reached, where the R^* , radius of the homogeneous nucleus, is equal to R . This critical undercooling is $\Delta T_c \approx 2\gamma_{SL}/(\Delta s_f R)$. Here Δs_f is the volumetric entropy of fusion. For larger undercoolings free growth sets in. This approach has been worked out for various shapes of the foreign particles.¹⁷ This simple concept proved highly successful in various branches of science ranging from materials science to cryobiology,¹ where particle induced freezing occurs.

1.3 Problems with the classical theory

While the pre-exponential factor for the nucleation rate, the classical theory predicts, is reasonably accurate for vapor condensation and crystal nucleation, the sharp interface assumption used in the droplet model is reasonable only for nuclei that are much larger than the interface thickness. Under typical conditions the droplet model fails.¹⁸ Molecular dynamics indicate that the interface thickness is in the range of about 3 molecular diameters.^{19,20} Since at practically achievable largest undercoolings, where one might expect homogeneous nucleation, the critical size is comparable to this, it is probable that there are no bulk crystal properties at the center of the nuclei. Furthermore, it appears that even homogeneous nucleation is often a two-step process:^{21–23} the first appearing “precursor” state differs from the stable crystalline phase; it may be another crystalline structure (bcc^{9,23,24}), a dense liquid,^{25–27} or amorphous/disordered solid.^{28–32} The formation of the stable crystalline phase is assisted by the first forming precursor structures. In the case of heterogeneous nucleation, molecular scale studies indicate that the structure of the substrate plays an essential role.^{33–37} These complexities cannot be easily incorporated into the CNT.

In the following sections, phase-field models are reviewed that offer solutions to some of these problems.

2 Conventional Phase-Field Models

Van der Waals/Cahn-Hilliard/Ginzburg-Landau type continuum models^{38–40} have been used to model nucleation for a long time. These models are the earliest/simplest phase-field type approaches (they are also called simple classical density functional theories⁴¹). More complex approaches have been developed for describing solidification in multi-component/multi-phase/multi-domain problems.^{42–48}

2.1 Homogeneous nucleation

We start with illustrating the basic concepts of phase-field modeling of nucleation in a simple case, where a single structural order parameter ϕ monitors the structural transition between the liquid and the crystal. (Such an order parameter can be easily defined, when the number density of molecules in the crystal is approximated by a sum of Gaussian peaks, an assumption termed the quasi-harmonic approximation. Then the Fourier amplitudes of the number density in the crystal become expressible as $\phi = \phi_i (k_i/k_i)^2$.⁴⁹ Here ϕ_i is the i^{th} Fourier component, and k_i the respective

wave number. Accordingly, the dominant Fourier component ϕ_1 can be used as a structural order parameter.) The free energy can be expressed in terms of this order parameter and its spatial derivatives. In the respective phenomenological approach, the free energy can be written as

$$F = \int dV \left\{ \frac{\varepsilon^2}{2} |\nabla \phi|^2 + w g(\phi) + p(\phi) \Delta f \right\}, \quad (3)$$

where the form $g(\phi) = \frac{1}{4} \phi^2(1-\phi)^2$ and $p(\phi) = \phi^3(10 - 15\phi + 6\phi^2)$ are the double-well and interpolation functions (see Fig. 2), and Δf is the thermodynamic driving force of crystallization. As usual, the order parameter is 0 in the liquid and 1 in the crystalline phase. [Note that $g(\phi)$ and $p(\phi)$ functions can be taken from the Landau theory, but are often deduced from other principles.] Here, the free energy has three model parameters, ε^2 , w , and Δf . The latter is 0 at the melting point, whereas the free energy and the thickness of the solid-liquid interface can be related to the model parameters as: $\gamma_{SL} = \{\varepsilon^2 w / (6\sqrt{2})\}^{1/2}$ and $d_{SL} = 2 \cdot \ln(9) \{2\varepsilon^2/w\}^{1/2}$. The latter refers to the interfacial layer defined by $0.1 \leq \phi \leq 0.9$. All the model parameters can be expressed in terms of measurable quantities.

The critical fluctuation (nucleus) is a saddle point of the free energy in the function space, therefore, its properties can be obtained by solving the Euler-Lagrange equation under the following boundary conditions: unperturbed undercooled liquid in the far field, while the field gradients are zero at the center due to symmetry reasons.⁵⁰ For the sake of simplicity, an isotropic interface free energy is considered (a reasonable approximation for metals). The Euler-Lagrange equations boil down to $\phi'' + \left(\frac{2}{r}\right)\phi' = (1/\varepsilon^2)\partial_f \partial_\phi$. Here stands for spatial differentiation (d/dr), while the boundary conditions take the form $\phi' = 0$ at $r = 0$, and $\phi = 0$ for $r \rightarrow \infty$. Inserting the solution into the free energy and integrating the excess free energy density relative to the far field value (for

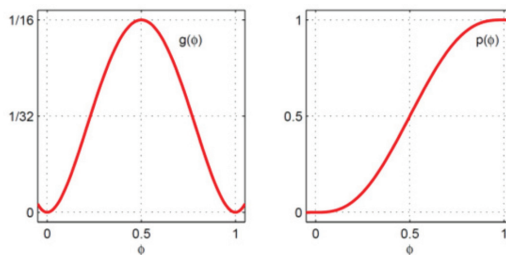


Figure 2: The form of the usual double-well and interpolation functions.

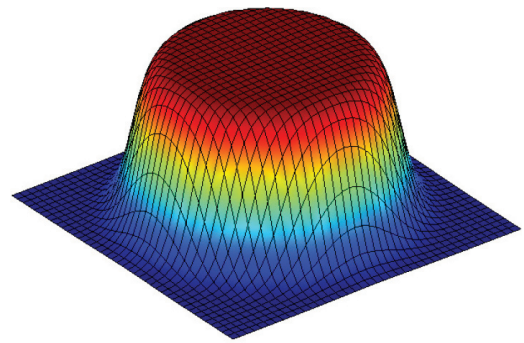


Figure 3: Phase-field distribution for the nucleus in two dimensions.

typical solutions see Fig. 3), one obtains nucleation barrier W_{hom}^* , which can be then plugged into the classical expression to obtain the nucleation rate. An advantage of this approach relative to the droplet model is that it considers that the solid-liquid interface is diffused (as shown by MD simulations), and that the non-bulk properties and the curvature dependence of the interface free energy are automatically handled. Remarkably, even this simple model leads to a considerable improvement in estimation of nucleation rate, especially if the structure related $g(\phi)$ and $p(\phi)$ from the Landau theory are used, as in the case of the hard-sphere system,^{51,52} competition of bcc and fcc nucleation in the Fe-Ni system.⁵³

2.2 Heterogeneous nucleation

To ensure heterogeneous nucleation, one needs to define a substrate within the framework of the phase-field model. There are two ways to do this: (a) a full phase-field representation of the substrate as a separate solid phase, which needs a detailed knowledge of the properties of the substrate (such as its free energy as a function of composition and temperature, solid-liquid and solid-solid the interfacial free energies, their anisotropies, the respective diffusion coefficients, etc.), and (b) if one has only the contact angle for the equilibrium trijunction, one may incorporate the respective substrate into the simulations via prescribing an appropriate boundary condition at its surface.

In fact, possibility (a) is automatically present in those phase-field models that consider the formation of two solid phases (e.g., eutectic or peritectic solidification), while nucleation of the phases is ensured by adding noise to the equations of motion. Examples for case (a) can be found in Refs. 54–58, though detailed analyses of the process is presented in Refs. 56–58, which explores the effect of fluid flow and anisotropy on the nucleation barrier.

Since case (b) is of broader practical interest, we briefly present the technique for heterogeneous nucleation on a flat surface in a simple binary system.⁵⁹ Accordingly, local state of the matter is described by a structural order parameter that monitors crystalline solidification [the phase field $\phi(\mathbf{r})$] and the concentration field $c(\mathbf{r})$ that represents the local composition. For the sake of simplicity, an isotropic solid-liquid interface is adopted again, which yields a cylindrically symmetric problem, i.e., the Euler-Lagrange equation is solved in cylindrical coordinates. Furthermore, no gradient term is assumed for the concentration in the free energy density. Under these circumstances, the Euler-Lagrange equation for the phase field reads as

$$\frac{1}{2} \frac{\partial}{\partial r} \left(r \frac{\partial \phi}{\partial r} \right) + \frac{\partial^2 \phi}{\partial z^2} = \frac{p'(\phi) \Delta f[\phi, c] + g'(\phi) w T}{\epsilon^2 T} \quad (4)$$

Owing to the absence of a $|\nabla c|^2$ term in the free energy density, the Euler-Lagrange equation for the concentration field defines a $c(\phi)$ relationship. As a result, the driving force for crystallization takes the form $\Delta f[\phi, c(\phi)] = f[\phi, c(\phi)] - (\partial f / \partial c)(c_\infty)[c(\phi) - c_\infty] - f_\infty$. Here, subscript ∞ denotes quantities referring to the initial liquid state. To ensure that in equilibrium (stable or unstable) the solid-liquid interface realizes a fixed contact angle ψ with the foreign wall placed at $z = 0$, we prescribe the following boundary condition at the wall⁵⁴ (a generalization of Model A in Refs. 60 and 61):

$$(\mathbf{n} \cdot \nabla \phi) = \sqrt{\frac{2\Delta f[\phi, c(\phi)]}{\epsilon^2 T}} \cos(\psi) \quad (5)$$

Here, the unit vector \mathbf{n} is the normal to the wall. This construction is easy to understand in the case of a stable triple junction, for which the contact angle is ψ . Owing to the presence of the wall, ordering takes place in a liquid layer of thickness d that extends to a few molecular layers (see e.g., Refs. 62 and 63). Taking $z = z_0 > d$, the equilibrium solid-liquid interface remains unperturbed by the wall (see Fig. 4). As a result, along the $z = z_0$ plane the phase-field and concentration profiles are related to the equilibrium profiles as in the equilibrium planar solid-liquid interface. Then, the following relationship holds

$$\frac{\epsilon^2 T}{2} \left(\frac{\partial \phi}{\partial n_{SL}} \right)^2 = \Delta f[\phi, c(\phi)] \quad (6)$$

Here n_{SL} is a spatial coordinate normal to the solid-liquid interface, whereas the component

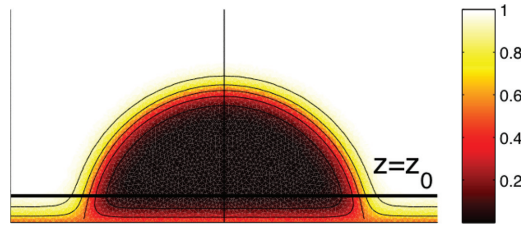


Figure 4: Typical cross-sectional phase-field map of a heterogeneous nucleus (computation performed with Model B of Refs. 60 and 61). Note the boundary layers between the wall and the bulk solid ($\phi = 0$ at the surface of the nucleus), and between the wall and the bulk liquid phase ($\phi = 1$ at the surface of the substrate). The crystal becomes disordered at the wall, whereas ordering of the liquid takes place at the wall. Above $z = z_0$ the solid-liquid interface remains essentially unperturbed by the presence of the wall. In the case of a stable tri-junction, the solid-liquid interface is planar (not curved as here for the nucleus).

of $\nabla \phi$ normal to the substrate wall is $(\mathbf{n} \cdot \nabla \phi) = (\partial \phi / \partial n_{SL}) \cos(\psi) = [2\Delta f / (\epsilon^2 T)]^{1/2} \cos(\psi)$. This means, e.g., that in the case of the parabolic groove approximation by Folch and Plapp,⁴⁵ one obtains $\Delta f[\phi, c(\phi)] = w T g(\phi)$.⁵³ Although Eq. (5) applies to the *equilibrium* trijunction, application of this approach for heterogeneous nuclei requires further considerations: The planar interface is not in equilibrium in the undercooled state, thus $\Delta f[\phi, c(\phi)]$ is a tilted double well, and Eq. (6) is not valid. In the case of the nucleus (being in unstable equilibrium), the capillary pressure restores the uniform chemical potential inside the nucleus. While, in principle, it would be possible to solve the appropriate spherical Euler-Lagrange equation for the phase field, and employ the respective solution to obtain the normal component $P_N(\phi)$ of the pressure tensor, which makes the chemical potential spatially uniform, it seems rather unpractical. However, a fairly good approximation can be obtained at least for large nuclei (small undercoolings) if Eq. (5) is used with $\Delta f' = \Delta f - [1 - p(\phi)] \cdot \Delta f_0$, where Δf_0 is the driving force of solidification. The latter correction term mimics the effect of capillary pressure as in equilibrium $\Delta f_0 = p_c$,⁶⁴ turning Δf into a double well of equal depths. Typical results obtained for heterogeneous nuclei in a binary system are shown in Fig. 5. Because of the relatively small undercooling applied here, the spherical cap model of the CNT is a good approximation for the height of the nucleation barrier.

Other methods have been worked out to ensure the contact angles, which rely on assuming a constant phase field or phase-field gradient at

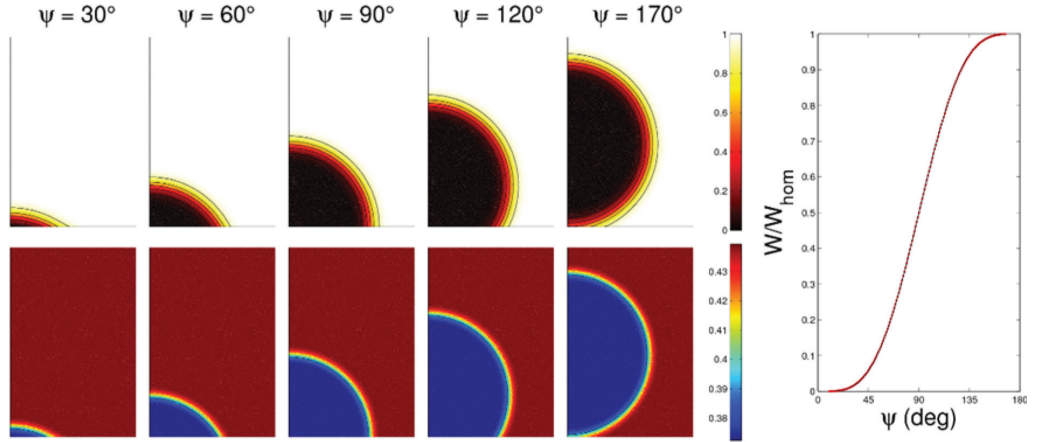


Figure 5: On the left: Phase-field (upper row) and concentration field (lower row) distributions for heterogeneous nuclei obtained solving numerically the Euler-Lagrange equations using the properties of a Cu-Ni alloy at 1574 K, while varying the contact angle, ψ . The computations were performed in a 100 nm \times 150 nm window. The contour lines (in upper row) denote phase field levels of $\phi = 0.1, 0.3, 0.5, 0.7$, and 0.9. The parabolic groove approximation by Folch and Plapp⁴⁵ was used to approximate the free energy. The model parameters were chosen so that the interface thickness is $d_{\text{SL}} = 1.76$ nm, whereas the solid-liquid interfacial free energy is $\gamma_{\text{SL}} = 0.3623$ J/m². On the right: The ratio of the barrier heights for the heterogeneous and homogeneous nuclei (termed as catalytic potency factor) is shown for the classical spherical cap model (black) and for the phase-field theory (red). The agreement between CNT and the phase-field results follows from the large size of nuclei ($R \gg d_{\text{SL}}$), where R the radius of curvature for the spherical cap.

the surface of the substrate (Models B and C in Refs. 60 and 61). Both of these approaches yields a surface spinodal, i.e., a critical undercooling beyond which free growth starts from the surface of the substrate.

2.3 Non-classical prefactor

While the pre-exponential factor the CNT predicts is reasonably accurate, efforts have been made to derive it from more fundamental theory.⁶⁵ A hydrodynamic theory of nucleation has been developed for vapor condensation⁶ and crystallization.²⁷ In both cases, the results appear to be rather close to the predictions of the classical theory.

2.4 Phase-field simulations of nucleation

One can perform *phase-field simulations for nucleation*, via adding a noise ζ to the equation of motion (EOM) as shown in Eq. (4), where noise needs to satisfy the fluctuation-dissipation theorem.

$$\frac{\partial \phi}{\partial t} = -M_\phi \frac{\delta F}{\delta \phi} + \zeta_\phi. \quad (7)$$

Here $\delta F/\delta \phi$ is the functional derivative of the free energy with respect to the phase-field, while the noise is assumed to have the correlator

$\langle \zeta(t, \mathbf{r}) \zeta(t', \mathbf{r}') \rangle = 2M_\phi kT \delta(t-t') \delta(\mathbf{r}-\mathbf{r}')$. An example of such phase-field simulations that illustrates the *free growth limited mechanism* mentioned above is shown in Fig. 6. Here the contact angles have been set via appropriate boundary conditions at the surfaces of the substrate.

2.5 Nucleation vs microstructure

Another important problem is, how one should incorporate homogeneous/heterogeneous nucleation into phase-field simulations. A possible solution is to add noise that satisfies the fluctuation-dissipation theorem to the equations of motion of the phase-field model as often done in the case of the time-dependent Ginzburg-Landau approach.^{50,54-57} This is another way to treat nucleation on the basis of the free energy functional. The major advantage of this approach is that nucleation happens automatically while considering the dynamics of the system. It is worth mentioning, however, that the addition of noise influences the position and depth of the free energy minima, and the magnitude of the interfacial free energy (via the capillary waves), etc.⁶⁶ If one wishes to retain the position of the minima and the interfacial free energy, a renormalization of the model parameters is needed. Another problem is that

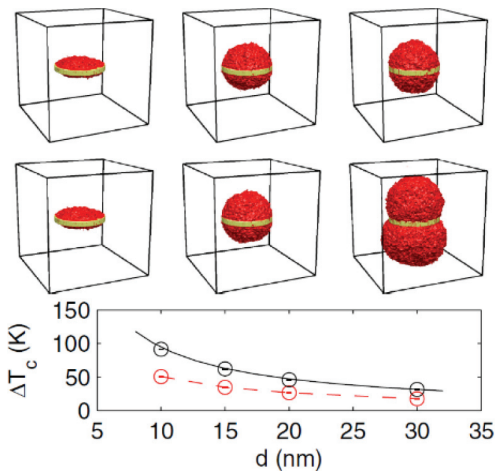


Figure 6: Free growth limited mode of particle induced crystallization as predicted by the phase-field theory for pure Ni.⁶⁰ The foreign particles were assumed to have a cylindrical shape of diameter $d = 20$ nm, whereas the contact angles on the horizontal and vertical surfaces were of 45° and 175° . Upper row: $\Delta T = 26$ K $< \Delta T_c$. Central row: $\Delta T = 27$ K $> \Delta T_c$. Time elapses from left to right. Bottom row: ΔT_c vs particle diameter d . Original theory — solid line; phase-field simulation — dashed line. The reduced ΔT_c observed in the simulations is due to the thermal fluctuations considered. (Reprinted with permission from L. Gránásy et al., *Phys. Rev. Lett.* 98, Art. no. 035703 (2007) © 2007 American Physical Society).

sub-nanometer resolution is required for this kind of simulations. It restricts the simulations to nanometer scale and very short times, in other words, to large undercoolings. Indeed, three dimensional simulations with sub-nanometer resolution are troublesome even for the largest supercomputers. To avoid this limitation for crystal growth for size scales that are much larger than the nuclei, a broad interface and large spatial steps have been adopted, while introducing appropriate choice for the interpolating functions and the ‘anti-trapping currents’, which remove the artifacts associated with the broad interfaces, including the overestimated solute trapping.^{67,68} Unfortunately, this cannot help nucleation, since normally the optimum size of the simulation cells for growth is orders of magnitude larger than the nuclei. To circumvent these practical problems, various techniques have been adopted. A possibility is to place randomly supercritical (larger than critical) clusters into the simulation window so that they realize the required nucleation rate. Details of this approach is described in Ref. 69.

2.5.1 Accelerating noise induced nucleation:

One may compute the nucleus and the nucleation rate by solving the Euler-Lagrange equation.⁵⁰ The nuclei can be placed spatially randomly in the simulation window with the appropriate statistics to realize required nucleation rate. The rest happens automatically: adding noise to the equation of motion a fraction of the nuclei decay, while the others grow as decided by the interplay of the local phase-field fluctuations.

2.5.2 Quantitative phase-field simulations:

One of the major problems of phase-field modeling is that a sub-nanometer resolution is needed in the interface, whereas micrometers or even mm size objects need to be described in three dimensions, while the time scale of the processes to be addressed might be in the minute/hour range. Unfortunately, the respective numerical problem cannot be solved even with the largest supercomputers: Taking equidistant Angstrom scale resolution in only a $1 \mu\text{m}^3$ volume yields 10^{12} grid points. Advanced numerical methods such as adaptive mesh, can reduce the required computational resources significantly,⁷⁰ yet noise induced nucleation (requiring sub-nanometer resolution throughout the liquid domain) and micrometer scale dendrites cannot be realized in the same simulation. In the case of crystal growth Karma and coworkers worked out an efficient practical solution:^{67,68} one may use an enhanced interface thickness, and thus, large spatial and time steps in the computations and correct for the consequences, so that the solution of the sharp interface problem is recovered accurately. Such quantitative phase-field simulations reproduced the behavior of thermal dendrites in pure Ni.⁷¹ The spatial steps may be typically of the order of a tenth of a micrometer. Normally, the nuclei cannot be resolved on this scale. To incorporate nucleation into such quantitative phase-field simulation, one needs to compute first the nucleation rate consistently with the free energy functional [using the nucleation barrier from solving the Euler-Lagrange equation(s)⁵⁰ and the classical pre-exponential factor], then insert small crystal seeds of supercritical size (that are able to grow) randomly in space and time with the corresponding frequency.

2.5.3 Free growth limited model: This mechanism (see Section 1.2) can also be implemented similarly for sub- Δx particles: assign

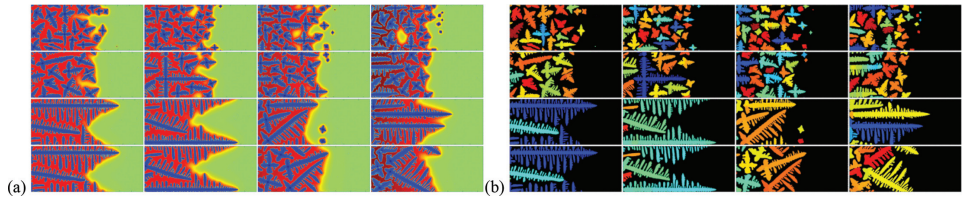


Figure 7: Columnar to equiaxed transition in an Al-Ti alloy as predicted by the phase-field theory.⁷² (a) The maps of concentration and (b) the maps of crystallographic orientation are shown for 16 simulations: From left to right: the temperature gradient is $Q = (5, 10, 20 \text{ and } 40) \times 10^4 \text{ K/m}$, respectively. From bottom to top: The pulling velocity is $V_0 = (4, 8, 16, \text{ and } 32) \times 10^{-4} \text{ m/s}$. A rectangular grid of size 1500×300 (corresponding to $0.75 \text{ mm} \times 0.15 \text{ mm}$) was used in the simulations (only half of the window is shown). At every instance about 200 nanoparticles were present in the simulation box, which had a Gaussian size distribution of average 20 nm, and standard deviation of 4 nm.

particles of given size distribution randomly to the pixels/voxels of the simulation, compute the respective critical undercoolings considering the local temperature and composition, and compare it with the actual undercooling. Once the latter becomes larger than the critical undercooling for the given particle, flip the phase-field from 0 to 1. As Δx is usually much larger than the critical size, this will initiate growth. Results from such a procedure are shown in Fig. 7.⁷² Kim's model⁴⁶ was used for an Al-Ti alloy. The thermodynamic data were taken from a refined assessment performed during the IMPRESS project.⁷² The material was made to move with a constant velocity $v_x = -V_0$ from right to left in the simulation window, while a constant temperature gradient Q was prescribed along the horizontal axis. Periodic boundary condition was applied along the horizontal boundaries, whereas liquid of fixed temperature and composition entered the box on the right, and the matter of the actual composition distribution left the box on the left side. In quantitative agreement with Hunt' theory, nucleation controlled equiaxed morphology appeared in the upper eight panels of Fig. 7, whereas columnar dendritic morphology formed in the lower eight panels.

A more detailed strategy for modeling the free growth limited mechanism is also possible that considers growth from the size of the foreign particle to the size of the pixel/voxel and the respective heat release.^{73–76}

2.5.4 Modeling growth front nucleation: Complex polycrystalline solidification morphologies, such as spherulites, crystal sheaves, and axialites, form via a process termed Growth Front Nucleation (GFN): i.e., by the appearance of new grains at the propagating solidification front.⁷⁷ Essential features of this phenomenon has been captured by phase-



Figure 8: Orientation map from a phase-field model of spherulitic solidification relying on an orientation field.^{78,79} The formation of orientation defects at the solid-liquid interface is shown that initiate new grains. Different colors correspond to different crystallographic orientations. Sharp changes in color stand for grain boundaries (coherent dislocation lines), whereas the orientation defects can be interpreted as bundles of dislocations. The liquid domain is black.

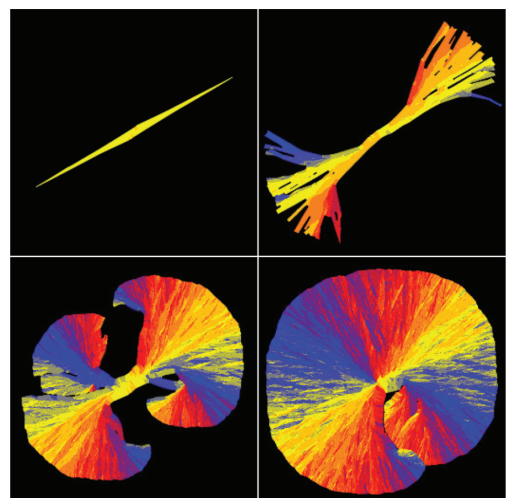


Figure 9: Transition from needle crystal to spherulite while varying the supersaturation in phase-field modeling.⁸⁰ The supersaturation increases from left to right and from top to bottom.

field methods relying on orientation fields, which describe the local crystallographic orientation.^{47,78–80} In these models, the new grains form either by quenching orientational defects (interpreted as bundles of dislocations) into the crystal (see Fig. 8),⁷⁸ or via branching in directions of low grain-boundary energies.⁷⁹ The orientation field models became fairly successful in capturing complex polycrystalline growth structures (Fig. 9).^{47,78–80} Although these models have implications regarding the microscopic events taking place during GFN, direct information on such microscopic aspects is scarce, and further studies are warranted.

3 Phase-Field Crystal Modeling of Nucleation

The phase field models mentioned in the previous section can provide only a coarse grained view of the nuclei, and their role in determining the microstructure. However, the molecular scale structural aspects of crystal nucleation can be best investigated within microscopic approaches. For example, important pieces of information were obtained from **molecular dynamics/Monte Carlo simulations**.^{23,26,28,31–38,81,82} A complementary approach, which is able to address larger systems and longer times on the molecular scale is the Phase-Field Crystal (PFC) model.^{83–87} (For a recent review on the application of the PFC model to condensed-matter phase transitions see Ref. 88.) It is a simple dynamical **density functional theory** of classical particles, in which the local state of matter is characterized by a time averaged particle (singlet) density, $\Psi(\mathbf{r}, t)$. Recently, the PFC method was applied to model crystal nucleation^{89–94} and growth under various conditions.^{84–88} This approach automatically includes several competing crystalline phases (bcc, hcp, and fcc),^{89,95} besides the homogeneous liquid and the glass phases.^{94,95} Recent versions of the PFC model are able to include other crystalline structures.^{86,87} In the early versions,^{83–96} the time evolution of the system is described by overdamped conservative (diffusive) dynamics, which is appropriate for modeling colloidal crystalline aggregation. Advantages of the PFC models are that they can address solidification and solid state transitions on a diffusive time scale,^{83–96} and are able to handle millions of particles relatively easily.^{88,89} To address the freezing of ordinary liquids, a hydrodynamic theory of solidification based on the PFC approach has been put forward.⁹⁸ It is termed here the HPFC theory. Other approaches that combine PFC with fluid flow^{99,100} have not yet been used to address crystal nucleation.

Since the PFC studies addressing homogeneous and heterogeneous nucleation have been reviewed recently,⁹⁴ we present only a few examples, in which the PFC model contributed to a better understanding of nucleation phenomena in undecooled/supersaturated liquids: In agreement with theoretical predictions,^{26,27} molecular scale simulations,³¹ and experiments on colloidal systems,^{28–30} simulations based on the PFC model indicate that crystal nucleation is a two-step process at large supersaturations/undercoolings: an amorphous precursor assists the formation of the crystalline phase.^{89,91,94} Utilizing the $V\Psi$ term in Eq. (8) for including crystalline substrates into the simulations, heterogeneous nucleation occurring on crystalline particles, and flat- and complex shaped walls were investigated.^{89,92} For example, it was found that the free growth limited mode of particle induced crystallization (described in Section 1.2) works well for nanoparticles.

Finally, earlier efforts relying on the PFC model with diffusive dynamics without adding fluctuations to the EOM have shown that the creation of new grains at a propagating front, a phenomenon known as Growth Front Nucleation, was only possible at supersaturations beyond the stability limit of the liquid phase. Unfortunately, in the presence of fluctuations this phenomenon could not be observed, as copious nucleation occurring in the unstable liquid suppresses growth front nucleation. In contrast, recent work relying on the HPFC theory indicates the formation of new grains at the solidification front inside the metastable liquid domain.

Before presenting the results, we briefly recall the essential features of these models.

3.1 Free energy functional¹⁰¹

In the PFC-type models, the local state is characterized by a time-averaged single-particle density, ρ . The *dimensionless free energy* of the system measured relative to a homogeneous reference fluid (of density $\rho_{\text{L,ref}}$) is written in the following form

$$\Delta F = \int d\mathbf{r} \left\{ \frac{\Psi}{2} \left[-\varepsilon + (1 + \nabla^2)^2 \right] \Psi + \frac{\Psi^4}{4} + V\Psi \right\}. \quad (8)$$

Here, $\Psi_\infty (\rho - \rho_{\text{L,ref}})/\rho_{\text{L,ref}}$ is the scaled density, ε the reduced temperature that can be related to physical properties such as the bulk moduli of the fluid and the crystalline phases taken at the reference density and temperature. To represent foreign crystals, a periodic potential V is introduced. The free energy expression for $V = 0$ was deduced^{84,102} from the early perturbative

Molecular dynamics: A computer simulation method that explores the motion of atoms or molecules while they interact with each other. For more see: Ref. 81.

Monte Carlo simulations: A stochastic method for the evaluation of mainly equilibrium averages by efficient sampling of the configuration space of the system. For more see Ref. 82.

Classical Density Functional Theory (CDFT): Statistical physical description of phase transitions relying on time averaged particle density in describing the local state of matter. For a review on the application of CDFT for crystallization see Ref. 41.

density functional theory of crystallization proposed by Ramakrishnan and Yussouff.¹⁰³

3.2 The Euler-Lagrange equation

Utilizing that the nuclei represent a *saddle point* of the free energy, the corresponding particle density distribution can be found by solving the **Euler-Lagrange Equation** (ELE)^{88,89,91,92,94}

$$\frac{\delta\Delta F}{\delta\Psi} = \left. \frac{\delta\Delta F}{\delta\Psi} \right|_{\Psi_0}. \quad (9)$$

Functional, Euler-Lagrange equation, functional derivative: For these notions see *calculus of variations*, a branch of mathematics that works with functionals ('function of functions'), applied in a broad range of physical problems, optimization, etc.

See e.g. Ref. 101.

Here $\delta\Delta F/\delta\Psi$ stands for the **functional derivative** of the free energy with respect to the scaled particle density, and Ψ_0 is the reduced particle density of the reference liquid. At the borders of the simulation box periodic boundary condition is assumed. Inserting the free energy into Eq. (9) and rearranging the terms, one obtains

$$\left[-\varepsilon + (1 + \nabla^2)^2 \right] (\Psi - \Psi_0) = -(\Psi^3 - \Psi_0^3). \quad (10)$$

In other words,^{90,93} a *simplified string method* was employed to find the nucleation barrier.

3.3 The diffusive equation of motion

In the PFC model^{83,84} the time evolution of the particle density distribution follows a conserved overdamped dynamics. The respective dimensionless Equation Of Motion (EOM) reads as

$$\frac{\partial\Psi}{\partial t} = \nabla \cdot \left\{ \nabla \frac{\delta\nabla F}{\delta\Psi} + \xi \right\}. \quad (11)$$

Here, ξ is a colored Gaussian flux noise of **correlator**¹⁰⁴ $\langle \xi_i(\mathbf{r}, t), \xi_j(\mathbf{r}', t') \rangle = -\alpha^2 \delta_{ij} \nabla^2 g(|\mathbf{r} - \mathbf{r}'|, \sigma) \delta(t - t')$, where α is the strength of the noise, whereas $g(|\mathbf{r} - \mathbf{r}'|, \sigma)$ is a high frequency cutoff function, which removes wavelengths that are smaller than the interatomic spacing (σ).

3.4 Hydrodynamic theory of solidification

Recently, several approaches have been put forward combining a molecular scale theory with hydrodynamics that rely on different levels of approximations.^{98–100} However, so far, only the HPFC model proposed by Tóth *et al.*⁹⁸ has been applied to nucleation problems. In developing the HPFC model, our starting point was *fluctuating*

nonlinear hydrodynamics as formulated in Ref. 105. In this approach, the momentum transport and mass continuity equations are written in the following form

$$\frac{\partial\mathbf{p}}{\partial t} + \nabla \cdot (\mathbf{v} \otimes \mathbf{p}) = \nabla \cdot [\mathbf{R}(\rho) + \mathbf{D}(\mathbf{v}) + \mathbf{S}] \quad (12)$$

$$\frac{\partial\rho}{\partial t} + \nabla \cdot \mathbf{p} = 0 \quad (13)$$

Here $\mathbf{p}(\mathbf{r}, t)$ is the momentum, $\rho(\mathbf{r}, t)$ the mass density, and $\mathbf{v} = \mathbf{p}/\rho$ the velocity. As shown by Salmon¹⁰⁶ the reversible stress tensor can take the form $\nabla \cdot \mathbf{R} = -\rho \nabla \cdot \{\delta\Delta F[\rho]/\delta\rho\} \approx -\rho_0 \nabla \cdot \{\delta\Delta F[\rho]/\delta\rho\}$, while ρ_0 a reference density, and $\mathbf{D} = \mu_s \{(\nabla \otimes \mathbf{v}) + (\nabla \otimes \mathbf{v})^T\} + [\mu_b - (2/3)\mu_s](\nabla \cdot \mathbf{v})\mathbf{I}$ the dissipative stress tensor, while \mathbf{S} is a stochastic momentum noise of correlator

$$\begin{aligned} \langle S_{ij}(\mathbf{r}, t), S_{kl}(\mathbf{r}', t') \rangle &= (2kT\mu_s) \times \\ &\left[\left(\delta_{ik}\delta_{jl} - \delta_{jk}\delta_{il} \right) + \left(\frac{\mu_b}{\mu_s} - \frac{2}{3} \right) \delta_{ij}\delta_{kl} \right] \\ &\delta(\mathbf{r} - \mathbf{r}')\delta(t - t'). \end{aligned} \quad (14)$$

Here μ_s and μ_b are the shear and bulk viscosities.

Since the hydrodynamic equations refer to coarse grained quantities, we apply coarse-grained momentum and density in computing the velocity: $\mathbf{v} = \hat{\mathbf{p}}/\hat{\rho}$ in the convective and dissipative terms. (For details see Ref. 98.)

3.5 Numerical solutions

In recent works, the Euler-Lagrange equation was solved numerically in 2D and 3D, using semi-spectral successive approximation scheme combined with the operator-splitting method. An efficient method to find the saddle point of the free energy surface is the simplified string method described in Refs. 90 and 93. Other possible methods for finding the saddle point are reviewed in Ref. 107. The diffusive equation of motion and the hydrodynamic equations can be solved using semi-implicit spectral scheme based on operator splitting.¹⁰⁸

3.6 Examples for modeling nucleation within the PFC and HPFC models

3.6.1 Two-step homogeneous nucleation: It has been found that crystal nucleation takes place in two steps in the PFC model: First an amorphous precursor forms, which assists the appearance of the crystalline (bcc) phase.^{88,89,91,94} Besides colloids, this phenomenon appears to be relevant for simple model systems such as the Lennard-Jones²⁵ and

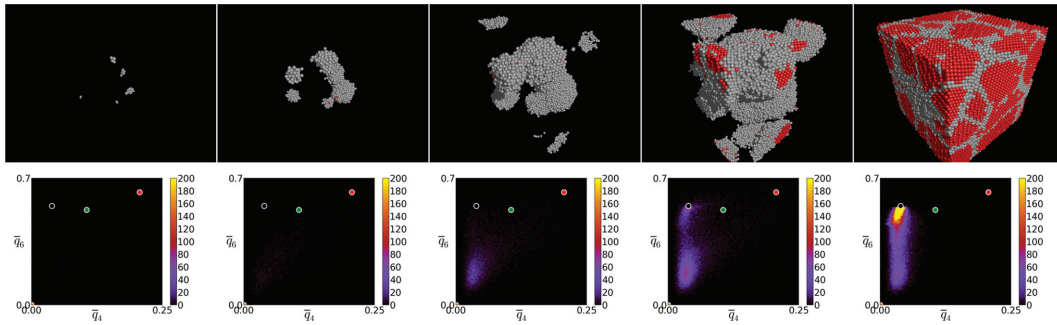


Figure 10: Two-step nucleation as predicted by the PFC model at $\varepsilon = 0.1684$ and $\psi_0 = -0.25$. Snapshots taken at dimensionless times $t = 20, 40, 60, 80$, and 200 , respectively are shown. **Upper row:** The density peaks are denoted by spheres colored to show the neighborhood: red (bcc-like neighborhood) $-q_4 \in [0.02, 0.07]$ and $q_6 \in [0.48, 0.52]$; white (amorphous)—the remaining particles. The liquid phase is made transparent. **Bottom row:** \bar{q}_4 vs. \bar{q}_6 bond-order parameter maps, as defined by Lechner and Dellago.¹¹⁰ These bond order parameters consider the first and second neighbors. The circles colored yellow, black, green, and red indicate the ideal icosahedral, bcc, hcp, and fcc structures, respectively.) These results imply that nucleation of amorphous domains initiate crystalline freezing.

hard-sphere³¹ fluids, implying that the presence of an amorphous precursor might be a general feature of crystal nucleation in highly undercooled or supersaturated fluids. Herein, we review the structural aspects of this process as predicted by the PFC model. We characterize the local structure using the **bond order parameters** q_i and \bar{q}_i as introduced by Steinhardt *et al.*¹⁰⁹ and Lechner and Dellago,¹¹⁰ respectively. Of them, q_i is evaluated using the molecule positions in the first neighbor shell around the particles, whereas in computing \bar{q}_i the q_i in the first neighbor shell are considered.

A two-step nucleation process was observed (Fig. 10), when quenching instantaneously a homogeneous liquid of reduced particle density $\psi_0 = -0.25$ from above the liquidus line ($\varepsilon = 0.1336$) to a highly undercooled state, $\varepsilon = 0.1667$. The noise strength employed was $\alpha = 0.42$. In the upper row of Fig. 10, the density peaks are indicated by molecule-size spheres that are colored red if they have a bcc-like neighborhood, whereas the rest of the molecules qualify amorphous, which are colored white. The liquid phase is not shown. The images showing solidification indicate that it starts by the formation of amorphous clusters, whereas the bcc structure appears later. The associated structural changes are displayed in the second row of Fig. 10, where the respective \bar{q}_4 vs. \bar{q}_6 bond order parameter maps are shown together with the points representing the ideal icosahedral, bcc, fcc, and hcp neighborhoods. The first appearing solid structure is an amorphous precursor represented by the blue halo appearing in the lower left corner. Its intensity (the amount of the amorphous neighborhoods) first increases with time, but reduces later as bcc crystallization takes over.

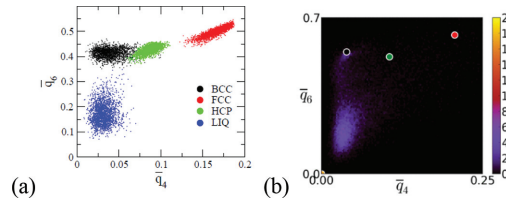


Figure 11: Comparison of the \bar{q}_4 vs. \bar{q}_6 bond-order parameter maps obtained (a) from molecular dynamics simulations for the liquid phase in the Lennard-Jones system (reproduced with permission from Ref. 110 © American Institute of Physics) and (b) for the solidifying PFC system (central panels of Fig. 1). Note the points for the ideal crystal structures in panel (b) fall higher than the ones obtained with thermal fluctuations in panel (a). Apparently, the structure of the amorphous precursor observed in the PFC model is close to the structure of the bulk liquid in the Lennard-Jones system.

Apparently, remnants of the amorphous structure stay at the grain boundaries even for rather long times. A comparison of the \bar{q}_6 vs. \bar{q}_4 bond-order parameter maps indicate that the structure of the amorphous precursor is similar to that of the bulk liquid observed in the Lennard-Jones system (see Fig. 11).

3.6.2 Heterogeneous nucleation on flat walls and particles: Utilizing the periodic potential term in Eq. 8, crystallization on various substrate geometries has been investigated in 2D and 3D. In the case of flat substrates of square lattice of varying lattice constant indicated that the contact angle and the nucleation barrier are non-monotonic functions of the lattice mismatch (Fig. 12).⁹² It was also shown that the free growth

Bond order parameters: They characterize the local structure around a given particle k . Steinhardt *et al.*¹⁰⁹ introduced the rotationally invariant bond order parameters

$$q_l^k = \left\{ \frac{4\pi}{2l+1} \sum_{m=-l}^l |q_{lm}|^2 \right\}^{1/2}.$$

Here

$$q_{lm}^k = 1/n_b^k \sum_{j=1}^{n_b^k} Y_{lm}(\mathbf{r}_{kj}),$$

while $Y_{lm}(\mathbf{r}_{kj})$ are the spherical harmonic functions of degree l , and order m , and n_b^k is the number of the bonds of particle k . More recently, Lechner and Dellago¹¹⁰ introduced a coarse-grained/average bond order parameter that is extended to the second neighbors:

$$\bar{q}_l^k = \left\{ \frac{4\pi}{2l+1} \sum_{m=-l}^l |\bar{q}_{lm}^k|^2 \right\}^{1/2},$$

and

$$\bar{q}_{lm}^k = 1/N_b^k \sum_{j=0}^{N_b^k} q_{lm}^j.$$

Here, the sum for j runs for all neighbors N_b^k of particle k including the particle itself. Thus, in computing the average \bar{q}_l^m for particle k , one uses the local orientational order vectors averaged over particle k and its surroundings. While q_k^l relies on structural information from the first shell around particle k , its averaged version \bar{q}_l^k structural information from the second shell is also taken into account. The spatial averaging has a tremendous significance in detecting local ordering with high sensitivity: Separation of the crystal structures is far more pronounced when using the average bond order parameters.

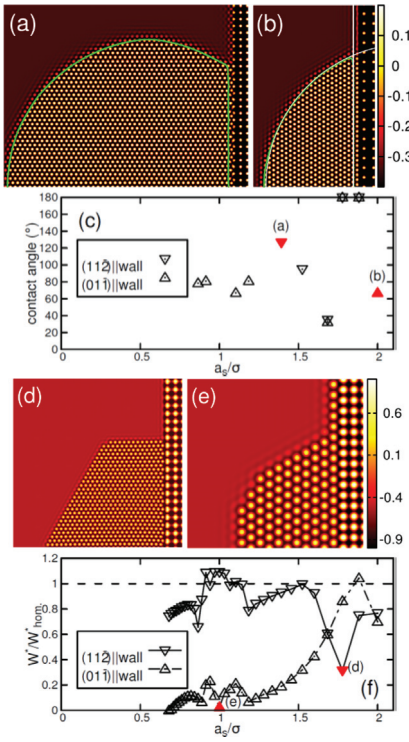


Figure 12: Heterogeneous crystal nucleation on a flat wall in 2D from solving ELE for a square lattice substrate.⁹² (a),(b) Typical non faceted nuclei occurring at small reduced temperatures. The lattice mismatch for the two panels are $a_s/\sigma = 1.49$ and 2.0 , respectively. Here a_s is the lattice constant of the substrate, whereas σ is the lattice constant of the nucleating crystal. (c) Contact angle versus the lattice mismatch. (d),(e) Faceted nuclei obtained far from the critical point, at $a_s/\sigma = \sqrt{3}$ and 1.0 . (f) Free energy of formation of faceted nuclei normalized by the value for homogeneous nucleation, W^*_{hom} .

limited model of particle induced nucleation is qualitatively valid for non-faceted crystals, small undercoolings, and large substrates. It was found, however, that the stable shape at the critical undercooling depends on the size of the foreign particle: in the case of a cubic substrate of simple cubic crystal structure it was found that for small nanoparticles (e.g., $L = 16a$, where a is the lattice constant of the bcc structure) pyramids form on the faces of the cube. For twice of this linear size, spherical caps evolve on the cube faces, whereas for larger sizes the shape computed using a surface solver¹⁷ applies (Fig. 13).

3.6.3 Modeling growth front nucleation: Here, we review recent results concerning the formation of new grains at the solid-liquid interface within the framework of molecular scale approaches such as the PFC and HPFC



Figure 13: Size dependence of the stable crystal shape that precedes free growth on square-shaped square-lattice substrates. From left to right: $L_s = 16\sigma$, $L_s = 32\sigma$, and theoretical shape for infinite size.¹⁷

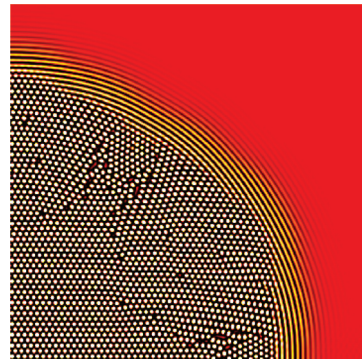


Figure 14: Formation of defects and new crystallographic orientations beyond the linear stability limit of the liquid in the original PFC model. Here noise was omitted ($\alpha=0$), the average density and the reduced temperature were $\psi_0 = -0.45$ and $\epsilon = 0.75$, respectively, whereas the stability limit was $\psi_c = -0.5^7$.

models. The first attempts to model GFN on the nanoscale were made using the original PFC model. Omitting noise, while working beyond the linear stability limit of the homogeneous liquid [$\psi > \psi_c = -(\epsilon/3)^{1/2}$], single crystal seeds evolved into symmetric polycrystalline structures (Fig. 14). Beyond the stability limit, the solid-liquid interface becomes broader: the growing crystal is surrounded by concentric density waves, which initiate crystallization accordingly. In six directions these waves assist the growth of the original crystallographic orientation. In other directions, however, a large number of defects form and new orientations appear that fit locally to the density waves (Fig. 14). Although this might be viewed as an elementary process for GFN, in this regime the liquid is unstable: adding noise to the EOM, these phenomena are suppressed by copious crystallization taking place in the unstable liquid domain. Inside the metastable liquid domain, we were unable to find GFN.

In contrast, in the case of the HPFC model, we were able to grow polycrystalline domains from a

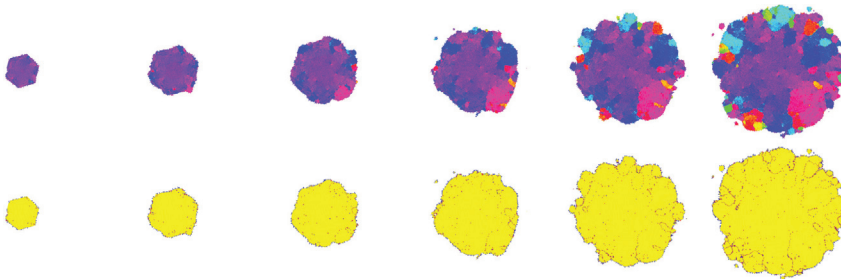


Figure 15: Polycrystalline growth from a single-crystal seed in a metastable liquid in the presence of momentum noise as predicted by the HPFC model. The dynamic equation were solved on a 4096^2 rectangular grid assuming periodic boundary condition at the borders of the simulation box. Snapshots taken at dimensionless times $t = 2000, 2500, 3000, 3500, 4000$, and 4500 are shown. The orientation maps are shown in the upper row. (Here different colors correspond to different orientations.) Results of the Voronoi polyhedral analysis are displayed in the bottom row: the polyhedra are colored blue, yellow, or red, if the number of nearest neighbors is 5, 6, or 7, respectively. Note the dislocations/grain boundaries built of blue-red pairs. Two types of GFN can be recognized: (i) the formation of dislocations at the corners and at the center of edges of the initially hexagonal crystal, and (ii) nucleation of differently oriented crystallites near the solid-liquid interface (emerging from the interference of the density waves at the interfaces).

single-crystal seed as shown in Fig. 15. (Materials properties given in Ref. 98 were used.) Other conditions applied were: reduced temperature $\varepsilon = -0.0923$ and initial density $\psi_0 = \psi_c - 0.11\Delta$, where $\Delta = \psi_c - \psi_L = 0.0028$, whereas the densities corresponding to the liquidus and the stability limit were $\psi_L = -0.1982$ and $\psi_c = -0.1754$, respectively. The dynamic equations were solved on a 4096^2 rectangular grid, while prescribing periodic boundary conditions on all sides. A complex order parameter $g_6 = \sum_j \exp\{6i\theta_j\}$ was used for the structural analysis. The summation went for the nearest neighbors; here θ_j stands for the angle of the vector pointing to the j^{th} neighbor in the laboratory frame. The magnitude of g_6 represents the degree of crystalline order in the neighborhood of the molecule, whereas the phase indicates the local crystallographic orientation. Orientation maps are shown in the upper row of Fig. 13. Voronoi analysis of the crystal was also performed (see bottom row in Fig. 13). The following coloring scheme was employed: Voronoi cells for particles with 4, 5, 6, and 7 neighbors were painted grey, blue, yellow, and red, respectively. The simulation was performed in the presence of noise in the metastable liquid domain. It was found that the crystal seed grows first as a single crystal, but gradually new orientations appear via two distinct mechanisms of GFN: (1) Dislocations enter the hexagonal crystal along its perimeter. These are probably misfit dislocations, however, further work is needed to prove this. (2) Small crystallites nucleate in the neighborhood of the solid-liquid interface, which emerge from the interference of differently oriented density waves

emanating from the solid-liquid interface. Work is underway to quantify these phenomena.

A possible explanation for the failure of the PFC model in producing GFN is that, in this case, a fast growth mode is present, characterized by a wide solid-liquid interface, in which healing of the dislocations can be relatively easy, avoiding, thus, the formation of dislocations at the perimeter of the growing crystal, thereby preventing GFN.

4 Summary

We have presented a limited review that concentrates on different aspects of phase-field modeling of homogeneous and heterogeneous crystal nucleation. It covers the following main areas:

- i. coarse grained phase-field models:
 - homogeneous nucleation
 - heterogeneous nucleation with given contact angle
 - particle induced solidification
 - nucleation in large scale phase-field simulation
 - nucleation vs. microstructures
 - growth front nucleation
- ii. molecular scale phase-field models:
 - amorphous precursor assisted nucleation
 - nucleation on a flat substrate
 - particle induced solidification
 - growth front nucleation

While this paper is, by no means, a full review of the area, it provides a fairly broad view of the results, possibilities, and the

techniques involved. It is expected to be useful for researchers working in various branches of natural sciences where crystal nucleation plays an important role.

Acknowledgments

This work has been supported by National Agency for Research, Development, and Innovation (NKFIH), Hungary under contract No. OTKA-K-115959, by the EU FP7 Collaborative Project “EXOMET” (contract no. NMP-LA-2012-280421, co-funded by ESA), and by the ESA MAP/PECS projects “MAGNEPHAS III” (ESTEC Contract No. 40000110756/11/NL/KML) and “GRADECET” (ESTEC Contract No. 40000110759/11/NL/KML).

Received 4 July 2016.

References

- Kelton, K.F. and Greer, A.L. *Nucleation in Condensed Matter*, Amsterdam, Elsevier (2010).
- Kashchiev, D. *Nucleation: Basic theory with applications*, Oxford, Butterworth-Heinemann (2000).
- Vehkämäki, H. *Classical nucleation theory in multicomponent systems*, Berlin, Springer (2006).
- Kelton, K.F. and Greer, A.L. Test of classical nucleation theory in a condensed system, *Physical Review B* **38**, 10089–10092 (1988).
- Gránásy, L. and James, P.F. Nucleation and growth in cluster dynamics: A quantitative test of the classical kinetic approach, *Journal of Chemical Physics* **113**, 9810–9821 (2000).
- Langer, J.S. and Turski, L.A. Hydrodynamics model of the condensation of a vapor near its critical point, *Physical Review A* **8**, 3230–3243 (1973).
- Bravina, L.V. and Zabrodin, E.E. Homogeneous nucleation: Comparison between two theories, *Physics Letters A* **233**, 423–429 (1997).
- Talanquer, V. and Oxtoby, D.W. Dynamical density functional theory of gas-liquid nucleation, *Journal of Chemical Physics* **100**, 5190–5200 (1994).
- ten Wolde, P.R., Ruiz-Montero and Frenkel, D. Numerical calculation of the rate of crystal nucleation in a Lennard-Jones system at moderate undercooling, *Journal of Chemical Physics* **104**, 9932–9947 (1996).
- Binder, K. Theory for the dynamics of ‘clusters’. II. Critical diffusion in binary systems and the kinetics of phase separation, *Physical Review B* **15**, 4425–4447 (1977).
- Mirold, P. and Binder, K. Theory for the initial stages of grain growth and unmixing kinetics of binary alloys, *Acta Metall* **25**, 1435–1444 (1977).
- Gránásy, L., Egry, I., Ratke, L. and Herlach, D.M. Diffuse interface model of bulk heterogeneous nucleation, *Scripta Metallurgica et Materialia* **31**, 601–606 (1994).
- Gránásy, L., Pusztai, T. and Hartmann, E. Diffuse interface model of nucleation, *Journal of Crystal Growth* **167**, 756–765 (1996).
- Christian, J.W. *Transformations in metals and alloys*, Oxford, Pergamon (1981).
- Greer, A.L., Bunn, A.M., Tronche, A., Evans, P.V. and Bristow, D.J. Modelling of inoculation of metallic melts: Application to grain refinement of aluminium by Al-Ti-B, *Acta Materialia* **48**, 2823–2835 (2000).
- Quested, T.E. and Greer, A.L. A thermal heterogeneous nucleation of solidification, *Acta Materialia* **53**, 2683–2692 (2005).
- Reavley, S.A. and Greer, A.L. A thermal heterogeneous nucleation of freezing: Numerical modelling for polygonal and polyhedral substrates, *Philosophical Magazine* **88**, 561–579 (2008).
- Auer, S. and Frenkel, D. Prediction of absolute crystallization rate in the hard-sphere colloids, *Nature* **409**, 1020–1023 (2001).
- Laird, B.B. and Haymet, A.D.J. The crystal/liquid interface: Structure and properties from computer simulations, *Chemical Reviews* **92**, 1819–1837 (1992).
- Davidchack, R.L. and Laird, B.B. Simulation of the hard-sphere crystal–melt interface, *Journal of Chemical Physics* **108**, 9452–9462 (1998).
- Erdemir, D., Lee, A.Y. and Myerson, A.S. Nucleation of crystals from solutions: Classical and two-step models, *Accounts of Chemical Research* **42**, 621–629 (2009).
- Gebauer, D., Kellermeier, M., Gale, J.D., Bergström, L. and Cölfen, H. Pre-nucleation clusters as solute precursors in crystallisation, *Chemical Society Reviews* **43**, 2348–2371 (2014).
- ten Wolde, P.R., Ruiz-Montero, M.J. and Frenkel, D. Numerical evidence for bcc ordering at the surface of a critical fcc nucleus, *Physical Review Letters* **75**, 2714–2717 (1995).
- Shen, Y.C. and Oxtoby, D.W. bcc symmetry in the crystal–melt interface of Lennard-Jones fluids examined through density functional theory, *Physical Review Letters* **77**, 3585–3588 (1995).
- Lutsko, J.F. and Nicolis, G. Theoretical evidence for a dense fluid precursor to crystallization, *Physical Review Letters* **96**, Art. no. 046102 (2006).
- ten Wolde, P.R. and Frenkel, D. Enhancement of protein crystal nucleation by critical density fluctuations, *Science* **277**, 1975–1978 (1977).
- Lutsko, J. F. A dynamical theory of nucleation for colloids and macromolecules, *J. Chem. Phys.* **136**, Art. no. 034509 (2012).
- Schöpe, H.J., Bryant, G. and van Megen, W. Two-step crystallization kinetics in colloidal hard/sphere system, *Physical Review Letters* **96**, Art. no. 175701 (2006).
- Zhang, T.H. and Liu, X.Y. How does a transient amorphous precursor template crystallization, *Journal of the American Chemical Society* **129**, 13520–13526 (2007).

30. Zhang, T.H. and Liu, X.Y. Nucleation: What happens at the initial stage? *Angewandte Chemie International Edition* **48**, 1308–1312 (2009).
31. Schilling, T., Schöpe, H.J., Oettel, M., Opletal, G. and Snook, I. Precursor-mediated crystallization process in suspensions of hard spheres, *Physical Review Letters* **105**, Art. no. 027501 (2010).
32. Jacobson, L.J., Hujo, W. and Molinero, V.A. Amorphous precursors in the nucleation of clathrate hydrates, *Journal of the American Chemical Society* **132**, 11806–11811 (2010).
33. Esztermann, A. and Löwen, H. Wetting of topographically structured surfaces by crystalline phases, *Journal of Physics: Condensed Matter* **17**, S429–S441 (2005).
34. van Teeffelen, S., Likos, C.N. and Löwen, H. Colloidal crystal growth at externally imposed nucleation clusters, *Physical Review Letters* **100**, Art. no. 108302 (2008).
35. van Meel, J.A., Sear, R.P. and Frenkel, D. Design principles for broad-spectrum protein-crystal nucleants with nanoscale pits, *Physical Review Letters* **105**, Art. no. 205501 (2010).
36. Wang, J., Horsfield, A., Lee, P.D. and Brommer, P. Heterogeneous nucleation of solid Al from the melt by Al₃Ti: Molecular dynamics simulation, *Physical Review B* **82**, Art. no. 144203 (2010).
37. Wang, J., Horsfield, A., Schwingenschlögl, U. and Lee, P.D. Heterogeneous nucleation of solid Al from the melt by TiB₂ and Al₃Ti: An *ab initio* molecular dynamics study, *Physical Review B* **82**, Art. no. 184203 (2010).
38. van der Waals, J.D. Thermodynamische theorie der capillariteit in de onderstelling van continue dichtheidsverandering, *Verhandelingen der Koninklijke Akademie van Wetenschappen le Amsterdam (1^e sectie) DI*, 1–56 (1893).
39. Cahn, J.W. and Hilliard, J.E. Free energy of a nonuniform system. III. Nucleation in a two-component incompressible fluid, *Journal of Chemical Physics* **31**, 688–699 (1959).
40. Hohenberg, P.C. and Halperin, B.I. Theory of dynamic critical phenomena, *Review of Modern Physics* **49**, 435–479 (1977).
41. Oxtoby, D.W. Density functional methods in the statistical mechanics of materials, *Annual Reviews in Materials Research* **32**, 39–59 (2002).
42. Chen, L.-Q. and Yang, W. Computer simulation of the domain dynamics of a quenched system with a large number of nonconserved order parameters: The grain-growth kinetics, *Physical Review B* **50**, 15752–15756 (1994).
43. Steinbach, I., Pezzola, F., Nestler, B., Seesselberg, M., Prieler, R., Schmitz, G.J. and Rezende, J.L.L. A phase field concept for multiphase systems, *Physica D* **94**, 135–147 (1996).
44. Kobayashi, R., Warren, J.A. and Carter, W.C. Vector-valued phase field model for crystallization and grain boundary formation, *Physica D* **119**, 415–423 (1998).
45. Folch, R. and Plapp, M. Quantitative phase-field modelling of two-phase growth, *Physical Review E* **72**, Art. no. 011602 (2005).
46. Kim, S.G. A phase-field model with antitrapping current for multicomponent alloys with arbitrary thermodynamic properties, *Acta Materialia* **55**, 4391–4399 (2007).
47. Gránásy, L., Rátkai, L., Szállás, L., Korbuly, B., Tóth, G.I., Környei, L. and Pusztai, T. Phase-field modeling of polycrystalline solidification: From needle crystals to spherulites, *Metallurgical and Materials Transactions* **45 A**, 1694–1719 (2014).
48. Tóth, G.I., Pusztai, T. and Gránásy, L. A consistent multiphase-field theory for interface driven multi-domain dynamics, *Physical Review B* **92**, Art. no. 184105 (2015).
49. Shen, Y.C. and Oxtoby, D.W. Nucleation of Lennard-Jones fluids: a density functional approach, *Journal of Chemical Physics* **105**, 6517–6524 (1996).
50. Gránásy, L., Börzsönyi, T. and Pusztai, T. Nucleation and bulk crystallization in binary phase field theory, *Physical Review Letters* **88**, Art. no. 206105 (2002).
51. Gránásy, L. and Pusztai, T. Diffuse interface analysis of crystal nucleation in hard-sphere liquid, *Journal of Chemical Physics* **117**, 10121–10124 (2002).
52. Tóth, G.I. and Gránásy, L. Crystal nucleation in the hard-sphere system revisited: A critical test of theoretical approaches, *Journal of Physical Chemistry B* **113**, 5141–5148 (2009).
53. Tóth, G.I., Morris, J.R. and Gránásy, L. Ginzburg-Landau-type multiphase field model for competing fcc and bcc nucleation, *Physical Review Letters* **106**, Art. no. 045701 (2011).
54. Elder, K.R., Drolet, F., Kosterlitz, J.M. and Grant, M. Stochastic eutectic growth, *Physical Review Letters* **72**, 677–680 (1994).
55. Drolet, F., Elder, K.R., Grant, M. and Kosterlitz, J.M. Phase-field modeling of eutectic growth, *Physical Review E* **61**, 6705–6720 (2000).
56. Emmerich, H. and Siquieri, R. Investigating heterogeneous nucleation in peritectic materials via the phase-field method, *Journal of Physics: Condensed Matter* **18**, 11121–11129 (2006).
57. Siquieri, R. and Emmerich, H. Morphology-dependent crossover effects in heterogeneous nucleation of peritectic materials studied via the phase-field method for Al-Ni, *Journal of Physics: Condensed Matter* **21**, Art. no. 404105 (2009).
58. Prestipino, S., Laio, A. and Tosatti, E. A fingerprint of surface-tension anisotropy in the free-energy cost of nucleation, *Journal of Chemical Physics* **138**, Art. no. 064508 (2013).
59. Pusztai, T., Tóth, G.I., Tegze, G., Környei, L., Bansel, G., Fan, Z. and Gránásy, L. Phase-field approach to polycrystalline solidification including heterogeneous and homogeneous nucleation, *Journal of Physics: Condensed Matter* **20**, Art. no. 404205 (2008).
60. Gránásy, L., Pusztai, T., Saylor, D. and Warren, J.A. Phase field theory of heterogeneous crystal nucleation, *Physical Review Letters* **98**, art. no. 035703 (2007).

61. Warren, J.A., Pusztai, T., Környei, L. and Gránásy, L. Phase field approach to heterogeneous crystal nucleation in alloys, *Physical Review B* **79**, art. no. 014204 (2009).
62. Webb III, E.B., Grest, G.S. and Heine, D.R. Precursor film controlled wetting of Pb on Cu, *Physical Review Letters* **91**, art. no. 236102 (2003).
63. Toxvaerd, S. Molecular dynamics simulation of heterogeneous nucleation at a structureless solid surface, *Journal of Chemical Physics* **117**, 10303–10310 (2002).
64. Gránásy, L. Semiempirical van der Waals/Cahn-Hilliard theory: size dependence of the Tolman length, *Journal of Chemical Physics* **109**, 9660–9663 (1998).
65. Langer, J.S. Statistical theory of the decay of metastable states, *Annals of Physics* **54**, 258–275 (1969).
66. Plapp, M. Remarks on some open problems in phase-field modelling of solidification, *Philosophical Magazine* **91**, 25–44 (2011).
67. Karma, A. and Rappel, W.-J. Phase-field method for computationally efficient modeling of solidification with arbitrary interface kinetics, *Physical Review E* **53**, R3017–R3020 (1996).
68. Karma, A. Phase-field formulation for quantitative modeling of alloy solidification, *Physical Review Letters* **87**, art. no. 115701 (2001).
69. Simmons, J.P., Shen, C. and Wang, Y. Phase field modeling of simultaneous nucleation and growth by explicitly incorporating nucleation events, *Scripta Materialia* **43**, 935–942 (2000).
70. Provatas, N., Goldenfeld, N. and Dantzig, J. Efficient computation of dendritic microstructures using adaptive mesh, *Physical Review Letters* **80**, 3308–3311 (1998).
71. Bragard, J., Karma, A., Lee, Y.H. and Plapp, M. Linking phase-field and atomistic simulations to model dendritic solidification in highly undercooled melts, *Interface Science* **10**, 121–136 (2002).
72. EU FP6 Integrated Project IMPRESS (Intermetallic Materials Processing in Relation to Earth and Space Solidification), 2008. <http://www.spaceflight.esa.int/impress/>, The thermodynamic data employed in the phase-field simulation for Al-Ti were taken from Witusiewicz, V.T., Bondar, A.A., Hecht, U., Rex, S. and Velikanova, T.Y. The Al–B–Nb–Ti system III. Thermodynamic re-evaluation of the constituent binary system Al–Ti, *Journal of Alloys and Compounds* **465**, 64–77 (2008).
73. Böttger, B., Eiken, J. and Steinbach, I. Phase field simulation of equiaxed solidification in technical alloys, *Acta Materialia* **54**, 2697–2704 (2006).
74. Böttger, B., Eiken, J. and Apel, M. Phase-field simulation of microstructure formation in technical castings—A self-consistent homoenthalpic approach to the micro–macro problem, *Journal of Computational Physics* **228**, 6784–6795 (2009).
75. Eiken, J. Phase-field simulation of microstructure formation in technical magnesium alloys, *International Journal of Materials Research* **101**, 503–509 (2010).
76. Apel, M., Eiken, J. and Hecht, U. Phase field models for heterogeneous nucleation: Application to inoculation in alpha-solidifying Ti-Al-B alloys, *European Physical Journal B* **223**, 545–558 (2014).
77. Magill, J.H. Review spherulites: A personal perspective, *Journal of Materials Science* **36**, 3143–3164 (2001).
78. Gránásy, L., Pusztai, T., Börzsönyi, T., Warren, J.A. and Douglas, J.F. A general mechanism of polycrystalline growth, *Nature Materials* **3**, 645–650 (2004).
79. Gránásy, L., Pusztai, T., Tegze, G., Warren, J.A. and Douglas, J.F. Growth and form of spherulites, *Physical Review E* **72**, art. no. 011605 (2005).
80. Hendlér, N., Mentovich, E., Korbuly, B., Pusztai, T. and Gránásy, L. Growth control of peptide-nanotube spherulitic films: Experiments and simulations, *Nano Research* **8**, 3630–3638 (2015).
81. Frenkel, D. and Smit, B. *Understanding molecular dynamics simulations*, 2nd ed. San Diego, Academic (2002).
82. Landau, D.P. and Binder K. *A Guide to Monte Carlo Simulations in Statistical Physics*, 3rd ed., Cambridge, Cambridge University Press (2009).
83. Elder, K.R., Katakowski, M., Haataja, M. and Grant, M. Modeling elasticity in crystal growth, *Physical Review Letters* **88**, art. no. 245701 (2002).
84. Elder, K.R., Provatas, N., Berry, J., Stefanovic, P. and Grant, M. Phase-field crystal modeling and classical density functional theory of freezing, *Physical Review B* **75**, art. no. 064107 (2007).
85. Wu, K.-A., Adland, A. and Karma, A. Phase-field-crystal model for fcc ordering, *Physical Review E* **81**, art. no. 061601 (2010).
86. Greenwood, M., Provatas, N. and Rotter, J. Free energy functionals for efficient phase field crystal modeling of structural phase transformations, *Physical Review Letters* **105**, art. no. 045702 (2010).
87. Ofori-Opoku, N., Fallah, V., Greenwood, M., Esmaili, S. and Provatas, N. Multicomponent phase-field crystal model for structural transformations in metal alloys, *Physical Review B* **87**, art. no. 134105 (2013).
88. Emmerich, H., Löwen, H., Wittkowski, R., Gruhn, T., Tóth, G.I., Tegze, G. and Gránásy, L. Phase-field-crystal models for condensed matter dynamics on atomic length and diffusive time scales: an overview, *Advances in Physics* **61**, 665–743 (2012).
89. Tóth, G.I., Tegze, G., Pusztai, T., Tóth, G. and Gránásy, L. Polymorphism, crystal nucleation and growth in the phase-field crystal model in 2D and 3D, *Journal of Physics: Condensed Matter* **22**, art. no. 364101 (2010).
90. Backofen, R. and Voigt, A. A phase-field crystal approach to critical nuclei, *Journal of Physics: Condensed Matter* **22**, art. no. 364104 (2010).
91. Tóth, G.I., Pusztai, T., Tóth, G. and Gránásy, L. Amorphous nucleation precursor in highly nonequilibrium fluids, *Physical Review Letters* **107**, art. no. 175702 (2011).

92. Tóth, G.I., Tóth, G., Pusztai, T., and Gránásy, L. Heterogeneous crystal nucleation: The effect of lattice mismatch, *Physical Review Letters* **108**, art. no. 025502 (2012).
93. Backofen, R. and Voigt, A. A phase field crystal study of heterogeneous nucleation—Application of the string method, *European Physical Journal Special Topics* **223**, 497–509 (2014).
94. Gránásy, L., Podmaniczky, F., Tóth, G.I., Tegze, G. and Pusztai, T. Heterogeneous nucleation of/on nanoparticles: A density functional study using the phase-field crystal model, *Chemical Society Reviews* **43**, 2159–2173 (2014).
95. Jaatinen, A. and Ala-Nissila, T. Extended phase diagram of the three-dimensional phase field crystal model, *Journal of Physics: Condensed Matter* **22**, art. no. 205402 (2010).
96. Berry, J., Elder, K.R. and Grant, M. Simulation of an atomistic dynamic field theory for monatomic liquids: Freezing and glass formation, *Physical Review E* **77**, art. no. 061506 (2008).
97. Berry, J. and Grant, M. Modeling multiple time scales during glass formation with phase-field crystals, *Physical Review Letters* **106**, art. no. 175702 (2011).
98. Tóth, G.I., Gránásy, L. and Tegze, G. Nonlinear hydrodynamic theory of crystallization, *Journal of Physics: Condensed Matter* **26**, art. no. 055001 (2014).
99. Praetorius, S. and Voigt, A. A Navier-Stokes phase-field crystal model for colloidal suspensions, *Journal of Chemical Physics* **142**, art. no. 154904 (2015).
100. Heinonen, V., Achim, C.V., Kosterlitz, J.M., Ying, S.-C., Lowengrub, J. and Ala-Nissila, T. Consistent hydrodynamics for phase field crystals, *Physical Review Letters* **116**, art. no. 024303 (2016).
101. Gelfand, I.M. and Fomin, S.V. *Calculus of Variations*, Translated by Silverman, R.A. Dover (2000).
102. van Teeffelen, S., Backofen, R., Voigt, A., and Löwen, H. Derivation of the phase-field-crystal model for colloidal solidification, *Physical Review E* **79**, art. no. 051404 (2009).
103. Ramakrishnan, T.V. and Yussouff, M. First-principles order-parameter theory of freezing, *Physical Review B* **17**, 2775–2794 (1979).
104. Ojalvo, J.G. and Sancho, J.M. *Noise in Spatially Extended Systems*, New York, Springer (1999).
105. Shang, B.Z., Voulgarakis, N.K. & Chu, J.-W. Fluctuating hydrodynamics for multiscale simulation of inhomogeneous fluids: Mapping all-atom molecular dynamics to capillary waves, *Journal of Chemical Physics* **135**, art. no. 044111 (2011).
106. Salmon, R. Hamiltonian fluid mechanics, *Annual Review of Fluid Mechanics* **20**, 225–256 (1988).
107. Zhang, L., Ren, W., Samanta, A. and Du, Q. Computational Modeling of Nucleation in Phase Transformations, Submitted to *NPJ Computational Materials Science*.
108. Tegze, G., Bansel, G., Tóth, G.I., Pusztai, T., Fan, Z. and Gránásy, L. Advanced operator splitting-based semi-implicit spectral method to solve the binary phase-field crystal equations with variable coefficients, *Journal of Computational Physics* **228**, 1612–1623 (2009).
109. Steinhardt, P.J., Nelson, D.R. and Ronchetti, M. Bond-orientational order in liquids and glasses, *Physical Review B* **28**, 784 – 805 (1983).
110. Lechner, W. and Dellago, C. Accurate determination of crystal structures based on averaged local bond order parameters, *Journal of Chemical Physics* **129**, art. no. 114707 (2008).



Frigyes Podmaniczky is a PhD student at the Budapest University of Technology and Economics, and works at the Wigner Research Centre for Physics, Budapest, Hungary. His research areas include the investigation of complex solidification problems within the phase-field crystal model, such as heterogeneous nucleation, growth front nucleation, heteroepitaxy, dendritic solidification, and determination of the anisotropy of the crystal-liquid interface.



Gyula Tóth is a postdoctoral fellow at the Department of Physics and Technology, University of Bergen, Norway, since 2014. After receiving his PhD degree in 2012 at the Budapest University of Technology and Economics, he started to work as a postdoctoral research fellow at the Wigner Research Centre for Physics, Budapest, Hungary. His main interest includes phase-field modeling of flow and transformation dynamics in multiphase-multicomponent systems, complex solidification problems, classical and dynamical density functional theories of crystallization, hydrodynamic descriptions of first order phase transitions, and advanced numerical techniques in solving highly nonlinear, coupled partial differential equations, and GPU programming.



Tamás Pusztai, DSc, received his PhD degree in 2000 at the Eötvös University, Budapest, Hungary. Since then he is working at the Institute for Solid State Physics and Optics of the Wigner Research Centre for Physics in Budapest. He received his DSc degree from the Hungarian Academy of Sciences in 2013. His research interest includes phase-field modeling of solidification and microstructure formation, with emphasis on heterogeneous nucleation and polycrystalline freezing.



László Gránásy, DSc., received his PhD degree in Solid State Physics at the Eötvös University (in 1982), Budapest, Hungary, and his CSc and DSc degrees at the Hungarian Academy of Sciences (in 1989 and 2004, respectively). He is the leader of the Computational Materials Physics Group at the Wigner Research Centre for Physics, Budapest, and is a Guest Professor at BCAST, Brunel University, Uxbridge, U.K. He is a member of the Academia Europaea since 2014. His recent field of interest is mathematical and numerical modeling of complex solidification microstructures using continuum models (including phase-field and classical density functional methods), with special emphasis on nucleation and polycrystalline freezing.

